Examination of the failure behaviour of wood with a short crack in the tangential–radial system by single-edge-notched bending test

by Cicilia Susanti

Submission date: 23-Mar-2023 09:13PM (UTC+0900)
Submission ID: 2044385675
File name: Jurnal_E.pdf (825.5K)
Word count: 4715
Character count: 23985

Engineering Fracture Mechanics 77 (2010) 2527–2536

Contents lists available at ScienceDirect

Engineering Fracture Mechanics

journal homepage: www.elsevier.com/locate/engfracmech

Examination of the failure behaviour of wood with a short crack in the tangential–radial system by single-edge-notched bending test

Cicilia Maria Erna Susanti, Tetsuya Nakao, Hiroshi Yoshihara *

Faculty of Science and Engineering, Shimane University, Nishikawazu-cho 1060, Matsue, Shimane 690-8504, Japan

ARTICLE INFO

Article history:
Received 29 September 2009
Received in revised form 11 May 2010
Accepted 16 May 2010
Available online 18 June 2010

Keywords:
Single-edge-notched bending test
Mode I stress intensity factor
Bending strength
Correction crack length

ABSTRACT

Single-edge-notched tests of a tangential–radial system were conducted on agathis specimens to analyze the failure behaviour of wood with a short crack. The nominal bending strength and mode I critical stress intensity factors of the specimens with various crack lengths were measured, and the influence of the crack length on these properties was examined. The nominal bending strength of the cracked specimens was significantly lower than that of a crack-free specimen, even when the crack was extremely short. This finding suggests that the fracture mechanics theory is essential for analyzing the failure behaviour of wood with a very short crack. However, the mode I critical stress intensity factor still depended on the crack length. When considering the fracture process zone developing at the crack tip, the critical intensity factor could be predicted effectively.

1. Introduction

Over the years, various studies of the fracture properties of wood have been conducted on the basis of the fracture mechanics theory. Many of these studies are discussed in recent reviews [1,2]. Most of them have used specimens with relatively long cracks. In contrast, it is difficult to find any study that examines the fracture properties of specimens with short cracks, perhaps because it is assumed that the theory of fracture mechanics does not apply to such materials. According to research on metals by Irwin et al. [3], the nominal strength value of a cracked specimen coincides approximately with its actual strength, which is measured using a crack-free specimen when the crack is shorter than a certain critical length. When the crack is longer than the critical length, the nominal strength decreases as the crack length increases; hence, fracture mechanics is useful for analyzing the strength behaviour of the materials with a long crack. This phenomenon is described in several texts about fracture mechanics and it is reasonable to assume that it can be widely applicable to other materials, although it is not clear whether it is applicable to wood.

In the present study, single-edge-notched bending (SENB) tests were conducted using specimens of agathis with varying crack lengths that were smaller than those adopted in several existing studies involving the single-edge-notched tension or bending tests [4–9]. The nominal bending strength and mode I critical stress intensity factor were analyzed on the basis of elementary beam theory and linear fracture mechanics theory, respectively. The results revealed the appropriate method for analyzing the failure and fracture behaviours of wood with short cracks.

2. Three-point single-edge-notched bending test analyses

Fig. 1 shows a schematic diagram of the three-point single-edge-notched bending (SENB) test. The specimen, which had a crack of length a at its centre, was supported with a span of S, and the load was applied at the mid-span. The crack length is defined as a. In this loading condition, the nominal bending stress σ_n is derived from the elementary beam theory as follows:

* Corresponding author. Tel.: +81 852 32 6508; fax: +81 852 32 6123.
E-mail address: yosihara@riko.shimane-u.ac.jp (H. Yoshihara).

0013-7944/$ - see front matter © 2010 Elsevier Ltd. All rights reserved.
doi:10.1016/j.engfracmech.2010.05.019

Nomenclature

a	crack length
a'	corrected crack length
B	beam width
E_x	Young's modulus in the vertical direction
E_y	Young's modulus in the horizontal direction
$f(a/W)$	crack geometry factor
F_x^i	nodal force at the crack tip in the x-direction
F_y^i	nodal force at the crack tip in the y-direction
G_I	mode I energy release rate
G_{xy}	shear modulus in the vertical–horizontal plane
K_I	mode I stress intensity factor
K_{Ic}	critical value of the mode I stress intensity factor
P	applied load
P_c	critical load for crack propagation
W	beam depth
x	vertical direction of the specimen
y	horizontal direction of the specimen
δ_x^i	relative crack face displacement between the nodes adjacent to the crack tip in the x-direction
δ_y^i	relative crack face displacement between the nodes adjacent to the crack tip in the y-direction
Δ	additional crack length
Δa	length in the x- and y-directions of the element at the delamination front
ν_{xy}	Poisson's ratio in the vertical–horizontal plane
σ_n	nominal bending stress

List of acronyms

FPZ	fracture process zone
SENB	single-edge-notched bending
VCCT	virtual crack closure technique

$$\sigma_n = \frac{3SP}{2BW^2}, \tag{1}$$

where B and W are the beam width and depth, respectively, and P is the applied load. This notation is applicable to crack-free specimens. When a crack-free specimen is bent, the failure-by-bending moment is induced when σ_n reaches its critical value σ_{nc}, which is usually defined as the bending strength of the material.

As described above, σ_{nc} is considered to be constant for short cracks [3]. For long cracks, however, σ_{nc} decreases with increasing crack length. Therefore, the fracture behaviour of a material with a long crack should be analyzed using the mode I stress intensity factor K_I or the energy release rate G_I, each of which is derived from fracture mechanics theory. The value of G_I can be determined using energy considerations and is mathematically well defined, while K_I is regarded as a localized parameter that is influenced by microstructural local anisotropy [10]. In terms of rigor, the measurement of G_I, which requires the load–deformation relation corresponding to the crack length, is preferable to that of K_I. A compliance calibration method in which the loading-line compliance/crack length relation is required, is usually adopted for measuring G_I by an SENB test. In SENB testing of specimens with a short crack, however, it is difficult to obtain this relation appropriately,

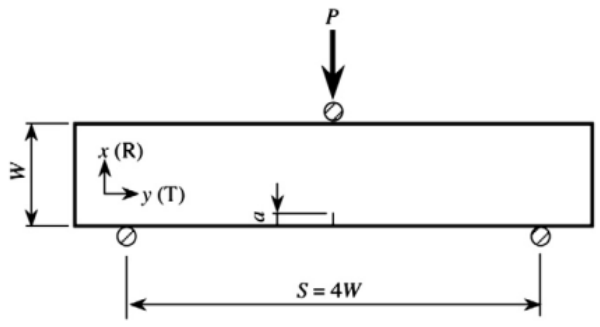

Fig. 1. Schematic diagram of the three-point single-edge-notched bending (SENB) test.

because the loading-line compliance does not vary with the crack length. In contrast, K_I, for which the load–deflection relation is not required, is more easily measured using an approximating equation than G_I is, despite being less mathematically rigorous.

The mode I stress intensity factor K_I is derived using the following equation:

$$K_I = \sigma_n \sqrt{\pi a} f\left(\frac{a}{W}\right), \tag{2}$$

where $f(a/W)$ is the crack geometry factor, which is usually determined by finite element method (FEM) calculations. The fracture is initiated when K_I reaches the critical stress intensity factor, defined as K_{Ic}, which is obtained by substituting σ_{nc} for σ_n in Eq. (2).

3. Finite element calculations

To determine the crack geometry factor $f(a/W)$, two-dimensional FEM calculations were performed using ANSYS version 11.0 from the Information Processing Center of Shimane University. Fig. 2 shows the finite element mesh of the SENB specimen. The depth of the models, W, had values of 15, 30 and 60 mm corresponding to the models with spans S of 60, 120 and 240 mm, respectively. Table 1 shows the crack length a used in the analyses, which are similar to those used in the actual SENB tests described in Section 4.3. The mesh was refined to be finer closer to the crack tip, as shown in Fig. 2b and c. Table 2 shows the elastic properties used in the calculations. These properties were determined by the vibration and compression tests described in Section 4.2. The vertical and horizontal directions of the model were defined as the x- and y-directions, respectively, and they corresponded to the radial and tangential directions of the wood. The crack was produced along the radial direction in the radial–tangential plane, which is the so-called TR system.

The models were supported in the vertical direction at y = 3, 6, and 12 mm and at y = 63, 126, and 252 mm for the models with depths of 15, 30, and 60 mm, respectively, and a vertical displacement u_x of 1 mm was applied at the node located at the top of the mid-span.

Mode I and mode II strain energy release rate components were calculated using the two-dimensional virtual crack closure technique (VCCT) [11] as follows:

$$\begin{cases} G_I = \frac{F_y^j \delta_y^i}{2B\Delta a} \\ G_{II} = \frac{F_x^j \delta_x^i}{2B\Delta a} \end{cases}, \tag{3}$$

where F_x^j and F_y^j are the nodal forces at the crack tip node j in the x- and y-direction, respectively. Also, δ_x^i and $\delta_x^{i'}$ are the relative displacements between nodes i and i', which are located at a distance Δa (=0.0125 mm) behind the crack tip in the x- and y-directions. In the calculations, the mode II strain energy release rate component was zero, therefore the fracture mechanics behaviours could be regarded as the pure mode I condition.

The value of G_I obtained by the VCCT was transformed into the mode I energy release rate K_I by the following equations [12]:

$$K_I = \sqrt{\frac{E_x G_I}{c_I}}, \tag{4}$$

where E_x is Young's modulus in the x-direction, and

$$c_I = \frac{1}{\sqrt{2}} \sqrt{\frac{E_x}{E_y}} \sqrt{\sqrt{\frac{E_x}{E_y}} + \frac{1}{2}\left(\frac{E_x}{G_{xy}} - 2\nu_{xy}\right)}, \tag{5}$$

where E_y is Young's modulus in the y-direction and G_{xy} and ν_{xy} are the shear modulus and Poisson's ratio in the xy-plane, respectively. The crack geometry factor $f(a/W)$ is derived from Eqs. (1), (2), and (4) as follows:

$$f\left(\frac{a}{W}\right) = \frac{2BW^2}{3SP\sqrt{\pi a}} \sqrt{\frac{E_x G_I}{c_I}}. \tag{6}$$

By substituting the total load applied to the finite element model P and G_I as calculated by the VCCT into this equation, the value of $f(a/W)$ corresponding to the equivalent crack length a/W was obtained.

4. Experiment

4.1. Materials

Agathis (*Agathis* sp.) lumber, with a density of 480 ± 10 kg/m^3 at 12% moisture content (MC), was used for the tests. When examining the fracture mechanics properties of the tangential–radial system, the influence of the annual rings is often

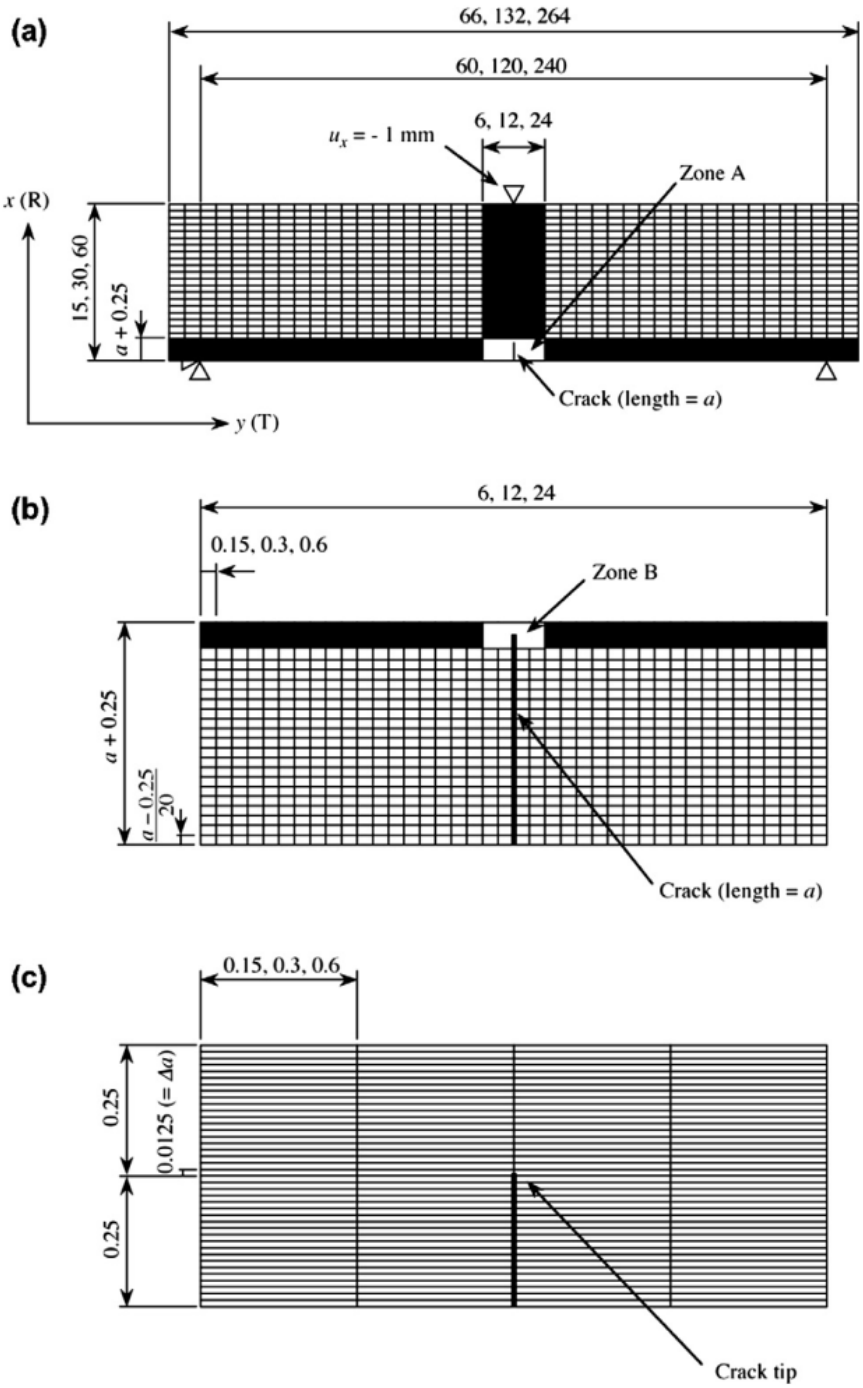

Fig. 2. Finite element model used for SENB test analysis: (a) overall mesh, (b) detail of zone A in (a) and (c) detail of zone B in (b). The crack length a is shown in Table 1.

significant [7]. Agathis is a tropical wood species without annual rings and so the influence of annual rings could be ignored in the analysis. The lumber had no defects such as knots or grain distortions, so that the specimens cut from it could be regarded as small and clear. The lumber was stored for several months in a room at a constant temperature of 20 °C and a relative humidity of 65% before the test and was confirmed to be in an air-dried condition. These conditions were maintained throughout the tests. The equilibrium MC was approximately 12%.

Table 1
Specimen configurations used for the SENB tests and finite element analyses.

Specimen type	Span S (mm)	Depth W (mm)	Width B (mm)	Crack length a (mm)
A	60	15	7.5	0, 0.5, 1, 2, 4, 5
B	120	30	15	0, 0.5, 1, 2, 4, 6, 9, 12
C	240	60	30	0, 0.5, 1, 2, 4, 8

Table 2
Elastic constants used for the finite element calculation.

E_x (GPa)	E_y (GPa)	G_{xy} (GPa)	ν_{xy}
0.87	0.68	0.14	0.45

x- and y-directions correspond to the radial and tangential directions of wood, respectively.

4.2. Compression and vibration tests for measuring the elastic constants

For the FEM analyses, Young's moduli in the radial and tangential directions, E_x and E_y, respectively, and the shear modulus (G_{xy}) and Poisson's ratio (ν_{xy}) in the radial–tangential plane are required. These constants were measured by compression and vibration tests.

E_x, E_y and ν_{xy} were measured by compression tests. A short-column specimen whose dimensions were 30 mm × 15 mm × 15 mm was prepared from the lumber described above. When E_x and ν_{xy} were measured, the long axis of the specimen coincided with the radial direction of the wood and coincided with the tangential direction when E_y was measured. Biaxial-strain gauges were bonded at the centres of the longitudinal–tangential planes, and a compression load was applied along the long axis of the specimen at a crosshead speed of 0.5 mm/min. From the stress–strain relationship in the loading direction, Young's moduli E_x and E_y were obtained. From the relationship between the loading and transverse strains, Poisson's ratio ν_{xy} was obtained.

The shear modulus in the radial–tangential plane G_{xy} was determined by free–free flexural vibration tests. A beam specimen whose dimensions were 15, 30 and 140 mm in the longitudinal, tangential and radial directions, respectively, was prepared. The specimen was suspended by threads at the nodal positions of the free–free resonance vibration mode and it was excited in the width direction using a hammer. The first to fourth resonance frequencies in bending were measured and analyzed by a fast Fourier transform (FFT) analysis program. The shear modulus G_{xy} was calculated by Hearmon's iteration method, the details of which are described in [13].

4.3. Single-edge-notched bending tests

All of the specimens were cut from the lumber described above so that they were long-matched to the dimensions shown in Table 1. For cracked specimens, the crack was produced along the radial direction in the TR system. The crack was first cut with a band saw (thickness = 1 mm); it was then extended ahead of the crack tip using a razor blade. The specimen was supported by the span shown in Table 1, and a load was applied to the specimen at a crosshead speed of 1 mm/min for the test with span lengths of 60 and 120 mm; a crosshead speed of 2 mm/min was used for the test with a span length of 240 mm. The test was conducted until the load markedly decreased.

Fig. 3 shows a typical load/loading-line deflection relation obtained by the SENB test. The crack always propagates unstably. If it propagated stably, the relation between the fracture toughness and crack propagation length (resistance curve, i.e. R-curve) could be obtained and the characteristics of the fracture mechanics could be evaluated by the R-curve [14,15]. Because of the unstable crack propagation, the R-curve could not be determined for any of the specimens tested here. Therefore, the fracture mechanics properties were evaluated from the load at the initiation of crack propagation. As demonstrated in Fig. 3, the load increases linearly until its maximum, and then drops immediately without displaying a nonlinear phase. As noted in previous studies [14,16], the loading-line compliance increases before the load reaches its maximum value because the fracture process zone (FPZ), a region of low stiffness, is produced ahead of the crack tip. Because of the FPZ, the effective crack length does not correspond to the initial crack length at peak load. Additionally, Dourado et al. pointed out that the real crack initiation occurred markedly after the peak load [17]. There are several definitions of the critical load for crack propagation [18]. Further studies should be conducted to determine the critical load and the effective crack length at the initiation of crack propagation. In this research, the load–deflection relation was linear and the crack propagated unstably, so the influence of the FPZ size was thought to be very small and the critical load for crack propagation, P_c, was determined as the maximum load. By substituting P_c into Eq. (1), the nominal bending strength σ_{nc} corresponding to crack length a was obtained. Then, the mode I critical stress intensity factor K_{Ic} corresponding to the crack length was obtained by substituting $f(a/W)$, which was determined by the finite element calculation and σ_{nc} into Eq. (2).

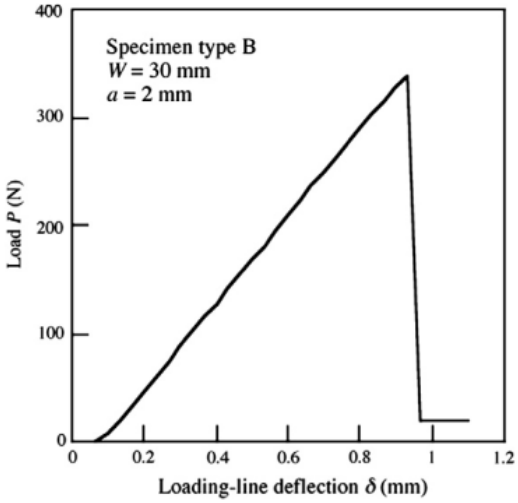

Fig. 3. Typical example of the load/loading-line deflection relation.

5. Results and discussion

5.1. Finite element analyses

Fig. 4 shows the relationship between the crack geometry factor $f(a/W)$ and the equivalent crack length a/W obtained by finite element calculation for the models with three different dimensions. In this figure, the polynomial relation derived for isotropic material [19], denoted as follows, is also represented.

$$f\left(\frac{a}{W}\right) = 1.09 - 1.735\left(\frac{a}{W}\right) + 8.20\left(\frac{a}{W}\right)^2 - 14.18\left(\frac{a}{W}\right)^3 + 14.57\left(\frac{a}{W}\right)^4 \tag{7}$$

There was a concern that the orthotropy of the wood might influence the crack geometry factor. However, Fig. 4 shows that the influence is so insignificant that Eq. (7) can be used as the crack geometry factor of this material. Hereafter, the mode I stress intensity factor is calculated using the crack geometry factor represented by Eq. (7).

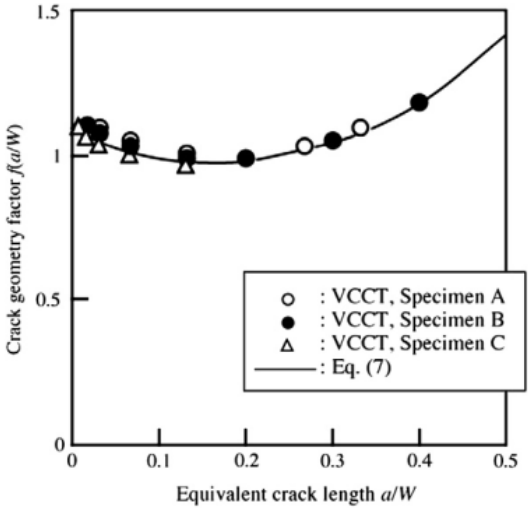

Fig. 4. Relationships between the crack geometry factor $f(a/W)$ and the equivalent crack length a/W obtained by the VCCT and Eq. (7) proposed by Gross and Srawley [15].

5.2. Three-point single-edge-notched bending tests

Fig. 5 shows the relationship between the nominal bending strength σ_{nc} and the crack length a. According to the results for metals [3], the nominal bending strength of a cracked specimen will approach the bending strength of a crack-free specimen when the crack length is decreased [3]. From the results obtained here, however, the value of σ_{nc} is markedly smaller than that of the crack-free specimen, and it decreases as the crack length increases. This suggests that fracture mechanics theory is essential for analyzing the failure behaviour of a cracked specimen even when the crack length is short.

Fig. 6 shows the relationship between the mode I critical stress intensity factor K_{Ic} and the crack length a. As already discussed, an analysis based on fracture mechanics is essential even when the crack is short. Nevertheless, the dependence of K_{Ic} on a is still significant for short cracks. According to previous studies [14–17,20–23], an FPZ in which the material softens progressively develops at the crack tip. Because of the FPZ, the cracked specimen often behaves as if the crack is longer than its actual length. The low stiffness in the FPZ usually induces an increase in the loading-line compliance [16,17,21]. As Fig. 3 shows, however, the nonlinearity in the load/loading-line deflection relation is not significant, so the dependence of K_{Ic} on a may not be attributed to FPZ production alone. Nevertheless, the dependence can be moderated by introducing an additional crack length Δ into Eq. (2):

$$K_I = \sigma_n \sqrt{\pi(a+\Delta)} f\left(\frac{a+\Delta}{W}\right) = \sigma_n \sqrt{\pi a'} f\left(\frac{a'}{W}\right), \tag{8}$$

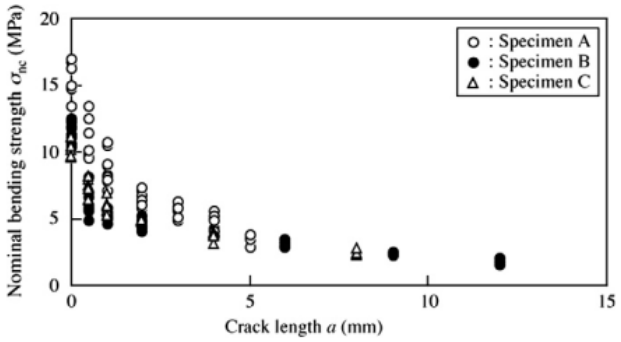

Fig. 5. Relationship between the nominal bending strength σ_{nc} and crack length a.

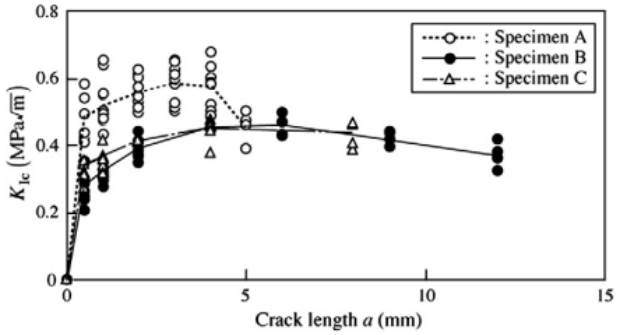

Fig. 6. Relationship between the mode I critical stress intensity factor K_{Ic} and crack length a.

Table 3
Additional crack length and additional equivalent crack length corresponding to each specimen type.

Specimen type	Additional crack length Δ (mm)
A	0.38
B	0.31
C	0.44

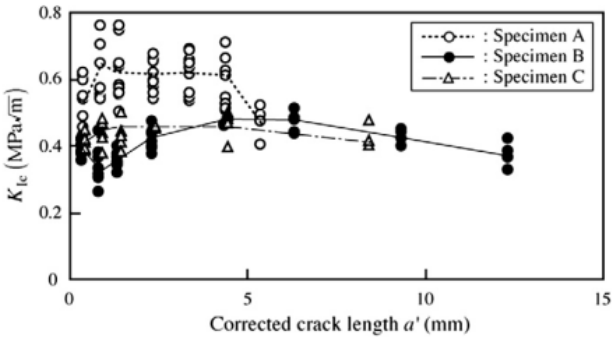

Fig. 7. Relationship between the mode I critical stress intensity factor K_{Ic} and corrected crack length a'.

Table 4
Mode I critical stress intensity factor K_{Ic} obtained with and without correcting the crack length.

Specimen type	K_{Ic} (MPa$\sqrt{m}$)	
	Crack length uncorrected	Crack length corrected
A	0.53 ± 0.07[a]	0.58 ± 0.07[d]
B	0.40 ± 0.04[b]	0.39 ± 0.05[d]
C	0.43 ± 0.03[c]	0.44 ± 0.04[d]

Results are averages ± SD. Crack length a used for obtaining K_{Ic}.
[a] 0.5, 1, 2, 3, 4 and 5 mm.
[b] 2, 4, 6, 9 and 12 mm.
[c] 2, 4 and 8 mm.
[d] All data including those at $a = 0$.

where a' is defined as the corrected crack length. Table 3 shows the value of the additional crack length Δ corresponding to each specimen type. The value of Δ was determined a follows: (1) the values of K_{Ic} were calculated under various values of Δ in Eq. (8), (2) the standard deviations of K_{Ic} corresponding to each crack length were obtained, and (3) the sums of the standard deviations, defined as s_D, corresponding to each Δ were obtained and compared. The value of Δ in Table 3 was determined as that from which the smallest value of s_D was derived. In previous studies [15,22,23], the value of Δ is physically determined based on the concept of the FPZ, and the validity is verified by finite element analyses. This method may be effective for determining the value of Δ. As previously noted, however, it is difficult to confirm that Δ is due to FPZ production alone. Therefore, the inverse method described above was adopted. Further research should be carried out to reveal the physical meaning of the additional crack length.

Fig. 7 shows the relationship between the mode I critical stress intensity factor K_{Ic} and the corrected crack length a'. With the crack-length correction, the dependence of K_{Ic} on the crack length is less significant than it is without the correction. Therefore, the crack-length correction is effective.

Table 4 shows the average values of K_{Ic} obtained with and without crack-length correction. As described above, K_{Ic} tends to be small when the crack is short and when the crack length is not corrected. Thus, the values shown in Table 4 are obtained by averaging the K_{Ic} values obtained for large crack lengths where the value of K_{Ic} is not dependent on the crack length. In contrast, the dependence of K_{Ic} on the crack length is less significant when the crack length is corrected, so K_{Ic} is obtained by averaging all data including those at $a = 0$. The relationships between σ_{nc} and a are predicted by substituting the values of K_{Ic}, a and $f(a/W)$ into Eq. (2), and K_{Ic}, a' and $f(a'/W)$ into Eq. (8). Fig. 8 compares the predicted and experimentally obtained σ_{nc}–a relationships. When the crack length is not corrected, the predicted strength increases markedly when the crack length approaches zero. When the crack length is corrected, however, the σ_{nc}–a relationship is predicted effectively over the full range of crack lengths, including when $a = 0$. Therefore, the failure behaviour is probably described by fracture mechanics theory even when the specimen has no crack.

As described above, the load/loading-line deflection relation does not represent the nonlinearity, so it is difficult to confirm that the additional crack length Δ is due to the FPZ alone because of the small value of Δ. From the experimental results obtained here, however, it is also difficult to identify the source of Δ definitively, so the value of Δ obtained here should be regarded as a correction of initial crack length. The anatomical structure of wood such as inherent cracks and cavities may have some influence on the value of Δ, and further researches including microscopic observation allow this phenomenon to be more clearly understood.

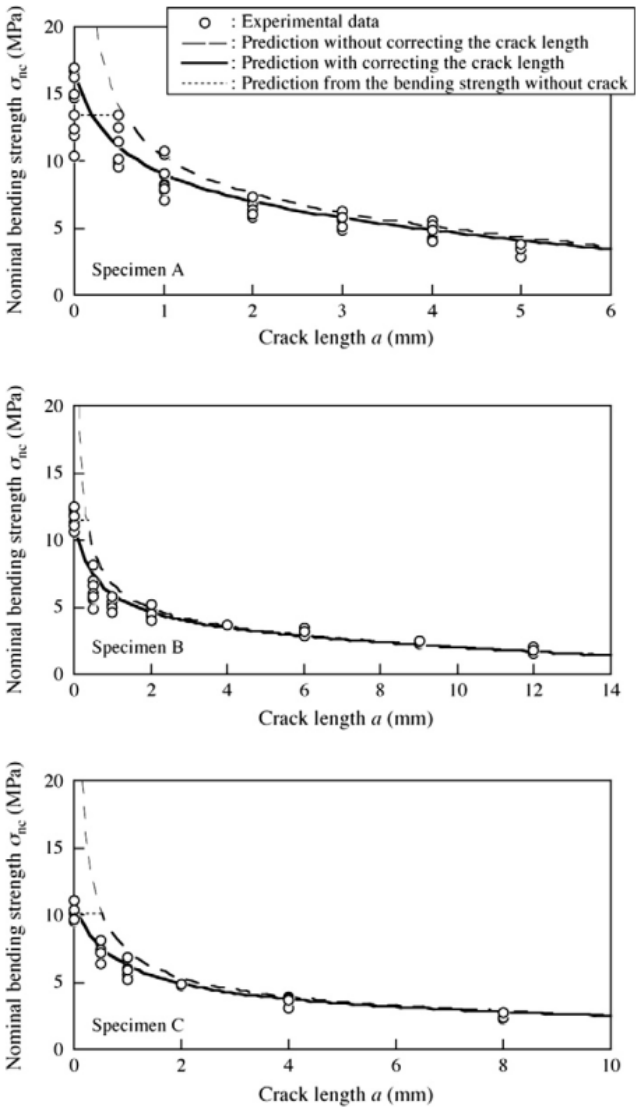

Fig. 8. Comparison of nominal bending strengths experimentally obtained and predicted on the basis of fracture mechanics theory.

6. Conclusion

Using specimens of agathis, SENB tests were conducted to analyze the failure behaviour of wood samples each containing a short crack.

According to previous study on metals conducted by Irwin et al. [3], crack length has little influence on the nominal bending strength when the crack is sufficiently short. In the experimental results obtained here, however, the nominal bending strength decreased with increasing crack length, and it was markedly lower than that of a crack-free specimen. Therefore, the fracture mechanics theory is essential for analyzing the failure behaviour of wood even when the crack length is very short.

The mode I critical stress intensity factor decreased when the crack length approached zero. With crack-length correction, however, the critical stress intensity factor was appropriately obtained over a wide range of crack lengths.

When the crack length was corrected, the relationship between the nominal bending strength and crack length was predicted effectively throughout the full range of crack lengths, even in the crack-free specimen.

Acknowledgements

The authors thank Mr. He Wen for his help in conducting the experiment. This study was partly supported by a Grant-in-Aid for Scientific Research (C) (No. 21580207) of the Japan Society for the Promotion of Science (JSPS).

References

[1] Conrad MPC, Smith GD, Fernlund G. Fracture of solid wood: a review of structure and properties at different length scales. Wood Fiber Sci 2003;35:570–84.
[2] Stanzl-Tschegg SE, Navi P. Fracture behaviour of wood and its composites. A review. Holzforschung 2009;63:139–49.
[3] Irwin GR, Kies JA, Smith HL. Fracture strength relative to onset and arrest of crack propagation. In: Proc ASTM, vol. 58; 1958. p. 640–57.
[4] Tribourlot P, Jodin P, Pluvinate G. Validity of fracture mechanics concepts applied to wood by finite element calculation. Wood Sci Technol 1984;18:51–8.
[5] Ashby MF, Eastering KE, Harrysson R. The fracture and toughness of woods. Proc Roy Soc Lond A 1985;398:261–80.
[6] Le-Ngoc L, McCallion H. On the fracture toughness of orthotropic materials. Engng Fract Mech 1997;58:355–62.
[7] Ando K, Ohta M. Variability of fracture toughness by the crack tip position of coniferous wood. J Wood Sci 1999;45:275–83.
[8] Wang L, Lu Z, Zhao G. Wood fracture pattern during the water adsorption process. Holzforschung 2003;57:639–43.
[9] Samarasinghe S, Kulasiri D. Stress intensity factor of wood from crack-tip displacement fields obtained from digital image processing. Silva Fenn 2004;38:267–78.
[10] Adams DF, Carlsson LA, Pipes RB. Experimental characterization of advanced composites materials. 3rd ed. Boca Raton: CRC Press; 2003.
[11] Rikards R, Buchholz FG, Wang H, Bledzki AK, Korjakin A, Richard HA. Investigation of mixed modes I/II interlaminar fracture toughness of laminated composites by using a CTS type specimen. Engng Fract Mech 1998;61:325–42.
[12] Sih GC, Paris PC, Irwin GR. On cracks in rectilinearly anisotropic bodies. Int J Fract Mech 1965;1:189–203.
[13] Hearmon RFS. The influence of shear and rotatory inertia on the free flexural vibration of wooden beams. Brit J Appl Phys 1958;9:381–8.
[14] Morel S, Bouchaud E, Schmittbuhl J. Influence of the specimen geometry on *R*-curve behavior and roughening of fracture surfaces. Int J Fract 2003;121:23–42.
[15] de Moura MFSF, Dourado N, Morais JJL. Crack equivalent based method applied to wood fracture characterization using the single edge notched-three point bending test. Engng Fract Mech 2010;77:510–20.
[16] Bažant ZP. Concrete fracture model: testing and practice. Engng Fract Mech 2002;69:165–205.
[17] Dourado N, Morel S, de Moura MFSF, Valentin G, Morais J. Comparison of fracture properties of two wood species through cohesive crack simulations. Composites A 2008;39:415–27.
[18] Davies P, Blackman BRK, Brunner AJ. Mode I delamination. In: Moore DR, Pavan A, Williams JG, editors. Fracture mechanics testing methods for polymers adhesives and composites, vol. 28. Amsterdam: ESIS Publication, Elsevier; 2001.
[19] Gross B, Srawley JE. Stress-intensity factors for three-point bend specimens by boundary collocation. NASA TN D-3092; 1965.
[20] Williams JG, Hadavinia H. Analytical solutions for cohesive zone models. J Mech Phys Solids 2002;50:809–25.
[21] Morel S, Dourado N, Valentin G, Morais J. Wood: a quasibrittle material *R*-curve behavior and peak load evaluation. Int J Fract 2005;131:385–400.
[22] de Moura MFSF, Morais JJL, Dourado N. A new data reduction scheme for mode I wood fracture characterization using the DCB test. Engng Fract Mech 2008;75:3852–65.
[23] de Moura MFSF, Campilho RDSG, Gonçalves JPM. Crack equivalent concept applied to the fracture characterization of bonded joints under pure mode I loading. Compos Sci Technol 2008;68:2224–30.

Examination of the failure behaviour of wood with a short crack in the tangential–radial system by single-edge-notched bending test

ORIGINALITY REPORT

35%	23%	32%	7%
SIMILARITY INDEX	INTERNET SOURCES	PUBLICATIONS	STUDENT PAPERS

MATCH ALL SOURCES (ONLY SELECTED SOURCE PRINTED)

3%

★ Hiroshi Yoshihara, Naoki Ataka, Makoto Maruta. "Measurement of the Young's modulus and shear modulus of extruded polystyrene foam by the longitudinal and flexural vibration methods", Journal of Cellular Plastics, 2016

Publication

Exclude quotes	On	Exclude matches	Off
Exclude bibliography	Off		